LA-UR- 98-2749

CONF-9806154--

TITLE: RECENT ADVANCES IN LATTICE BOLTZMANN METHODS

AUTHOR(S): Shiyi Chen, CNLS/T-Division
Gary D. Doolen, T-13/T-Division
Xiaoyi He, CNLS/T-Division
Xiaoblo Nie, CNLS/T-Division
Raoyang Zhang, CNLS/T-Division

SUBMITTED TO Proceedings: Conference on "National Congress of Applied Mechanics
June 20, 1998 to June 24, 1998 at Gaineville, FL

Los Alamos

Los Alamos National Laboratory
Los Alamos, New Mexico 87545

FORM NO. 836 R4
ST. NO. 2629 5/81

DISCLAIMER

Recent Advances in Lattice Boltzmann Methods

Shiyi Chen, Gary D. Doolen, Xiaoyi He, Xiaobo Nie and Raoyang Zhang
Center for Nonlinear Studies and Theoretical Division, Los Alamos National Laboratory, Los Alamos, NM 87545

In this paper, we briefly present the basic principles of lattice Boltzmann method and summarize recent advances of the method, including the application of the lattice Boltzmann method for fluid flows in MEMS and simulation of the multiphase mixing and turbulence.

I. INTRODUCTION

In recent years, the lattice Boltzmann method (LBM) [1] has emerged as an alternative and promising numerical scheme for simulating fluid flows and modeling physics in fluids. Unlike conventional numerical schemes based on discretizations of macroscopic continuum equations such as the Navier-Stokes equations, the lattice Boltzmann method is based on mesoscopic kinetic equations and the particle distribution function. The fundamental idea in the LBM is to construct simplified kinetic models that incorporate the essential mesoscopic physics so that the macroscopic averaged properties obey the desired macroscopic equations. By using a simplified version of the kinetic equation, one avoids solving complicated kinetic equations such as the full Boltzmann equation; and one avoids following each particle as in molecular dynamics simulations.

From the point of view of computational fluid dynamics, the kinetic nature of the LBM provides three important advantages. First, the convection operator in the LBM is linear allowing the incorporation of up-wind algorithms and avoiding the use of non-linear Riemann solvers. Simple convection combined with a relaxation process (or collision operator) allows the recovery of the nonlinear macroscopic advection through multi-scale expansions. Second, the incompressible Navier-Stokes equations are obtained in the nearly-incompressible limit of the LBM. This eliminates the necessity of solving the Poisson equation for the pressure, which is the normal procedure for solving the incompressible NS equations. Third, in contrast to traditional kinetic theory such as the continuum Boltzmann equation approach, the LBM seeks the minimum set of velocities in phase space. Only very a few velocities are used in the LBM, and the transformation relating the mesoscopic distribution function and macroscopic quantities, including mass, momentum and energy, is greatly simplified, consisting of simple arithmetic calculations.

The lattice Boltzmann equation for the discrete particle distribution function, similar to the kinetic equation in the lattice gas method [2], can be written as follows:

$$f_i(\mathbf{x} + \mathbf{e}_i\delta x, t + \delta t) - f_i(\mathbf{x}, t) = \Omega_i(f(\mathbf{x}, t)), \qquad (i = 0, 1 \cdots, M), \tag{1}$$

where f_i is the particle velocity distribution function along the ith direction; M is the number of particle speeds; $\Omega_i = \Omega_i(f(\mathbf{x}, t))$ is the collision operator which determines the rate of change of f_i due to collision. The most straightforward choice of collision operator is the linearized collision operator with a single relaxation time, τ, (or the BGK approximation [3,4]):

$$\Omega_i = -\frac{f_i - f_i^{(eq)}}{\tau}, \tag{2}$$

where $f_i^{(eq)}$ is the local equilibrium distribution function. Ω_i is required to satisfy conservation of total mass and total momentum at each lattice site in order to recover the NS equations:

$$\sum_i \Omega_i = 0, \qquad \sum_i \Omega_i \mathbf{e}_i = 0, \tag{3}$$

where $\sum_i \equiv \sum_{i=1,}^{M}$.

The macroscopic quantities, such as density, ρ, and momentum density, $\rho\mathbf{u}$, are defined as the particle velocity moments of the distribution function, f_i,

$$\rho = \sum_i f_i, \qquad \rho\mathbf{u} = \sum_i f_i \mathbf{e}_i, \tag{4}$$

It is assumed that the lattice spacing Δx and the time increment Δt in Eq. (1) can be treated as small parameters of the same order, ε. Performing a Taylor expansion in time and space, we obtain the following continuum form of the kinetic equation accurate to second order in ε,

$$\frac{\partial f_i}{\partial t} + \mathbf{e}_i \cdot \nabla f_i + \varepsilon(\frac{1}{2}\mathbf{e}_i\mathbf{e}_i : \nabla\nabla f_i + \mathbf{e}_i \cdot \nabla \frac{\partial f_i}{\partial t} + \frac{1}{2}\frac{\partial^2 f_i}{\partial t^2}) = \frac{\Omega_i}{\varepsilon}. \tag{5}$$

To derive the macroscopic hydrodynamic equation, we utilize the Chapman-Enskog expansion by assuming:

$$\frac{\partial}{\partial t} = \varepsilon\frac{\partial}{\partial t_1} + \varepsilon^2\frac{\partial}{\partial t_2}, \qquad \frac{\partial}{\partial x} = \varepsilon\frac{\partial}{\partial x_1}.$$

Likewise, the one-particle distribution function, f_i, can be expanded formally about the local equilibrium distribution function, f_i^{eq},

$$f_i = f_i^{eq} + \varepsilon f_i^{(neq)}. \tag{6}$$

Inserting the above formula into (5), we obtain, using simple algebra, the following mass and momentum equations:

$$\frac{\partial \rho}{\partial t} + \nabla \cdot \rho\mathbf{u} = 0, \tag{7}$$

$$\frac{\partial \rho\mathbf{u}}{\partial t} + \nabla \cdot \Pi = 0, \tag{8}$$

which are accurate to second order in ε. Here the momentum flux tensor, Π, has the form:

$$\Pi_{\alpha\beta} = \sum_i (\mathbf{e}_i)_\alpha (\mathbf{e}_i)_\beta [f_i^{eq} + (1 - \frac{1}{2\tau}) f_i^{(1)}]. \tag{9}$$

$(\mathbf{e}_i)_\alpha$ is the component of the velocity vector $\mathbf{e}_i$ in the α-coordinate direction.

To obtain the detailed form of Π, in the two-dimensional system we use a square lattice with nine speeds: $\mathbf{e}_i = (cos(\pi/4(i-1)), sin(\pi/4(i-1)))$ for $i = 1, 3, 5, 7$, $\mathbf{e}_i = \sqrt{2}(cos(\pi/4(i-1)), sin(\pi/4(i-1)))$ for $i = 2, 4, 6, 8$; $\mathbf{e}_0 = 0$ corresponds to a zero speed velocity. We also assume that the equilibrium distribution has the following form [4]:

$$f_i^{\text{eq}} = \rho w_i[1 + 3\mathbf{e}_i \cdot \mathbf{u} + \frac{9}{2}(\mathbf{e}_i \cdot \mathbf{u})^2 - \frac{3}{2}u^2], \tag{10}$$

with $w_0 = 4/9$, $w_1 = w_3 = w_5 = w_7 = 1/9$, and $w_2 = w_4 = w_6 = w_8 = 1/36$.

Inserting the above formula into (9), we obtain the resulting momentum equation

$$\rho(\frac{\partial \mathbf{u}_\alpha}{\partial t} + \nabla_\beta \cdot \mathbf{u}_\alpha \mathbf{u}_\beta) = -\nabla_\alpha p + \nu \nabla_\beta \cdot (\nabla_\alpha \rho \mathbf{u}_\beta + \nabla_\beta \rho \mathbf{u}_\alpha), \tag{11}$$

which is exactly as the same as the Navier-Stokes equation if the density variation $\delta\rho$ is small.

II. LBM SIMULATION OF FLOWS IN MEMS

The LBM has been widely used for simulating fluid flows, including complex flows, fluid turbulence, suspension flows and reaction diffusion systems (see the review [1]). Most of the applications are related to flows in the incompressible limit whose dynamics can be described by the macroscopic Navier-Stokes equations. Since the lattice Boltzmann method is intrinsically kinetic, it is more general and can be used to simulate fluid flows with mean-free-path effects associated with high Knudsen numbers, such as fluid flows in MEMS [5]. In this section we present LBM simulation results for flows in a micro-channel [6].

For flows in a micro-channel, the mean free path of fluid molecules could be the same order as the typical geometric length of the device or larger. The continuum hypothesis which is fundamental for the Navier-Stokes equation breaks down. An important feature in these flows is the emergence of a slip velocity at the flow boundary, which strongly affects the mass and heat transfer in the system. In our LBM simulation, the micro-channel consists of two parallel plates separated by a distance h and the fluid flow is driven by the pressure difference between the inlet pressure, P_i, and exit pressure, P_e. The channel length in the longitudinal direction is L. The bounce-back boundary condition [1] is used for the particle distribution functions at the plates (i.e., when a particle distribution hits a wall node, the particle distribution scatters back to the fluid nodes in a direction opposite to its incoming direction). The Knudsen number is defined as $K_n = l/h$, where l is the mean free path of the fluid molecular.

The slip velocity V_s at the exit of the micro-channel is determined using the following formula:

$$u(y) = u_0(Y - Y^2 + V_s), \tag{12}$$

where $u(y)$ is the velocity along the flow direction at the exit and $Y = y/h$. u_0 and V_s can be obtained by fitting numerical results using the least squares method.

In Fig. 1, we plot the slip velocity V_s and the normalized mass flow rate $M_f = M/M_0$ as functions of Knudsen number when the pressure ratio $\eta = P_i/P_e = 2$. The normalization

factor, $M_0 = \frac{h^3 P_e}{24\nu}(\eta - 1)$, is the mass flow rate when the velocity slip is zero. Using a least squares fit, from Fig. 1 we obtain:

$$V_s = 8.7K_n^2. \tag{13}$$

If we assume that the Navier-Stokes equation is valid for the micro-flow except that the slip boundary condition V_s in Eq.(13) is used to replace the traditional non-slip condition on walls (the similar procedure has been used in the engineering model [7]), Eqs. (11) and (13) give the analytical mass flow rate:

$$M_f = 1 + 12V_s(K_n)\frac{\ln(\eta)}{\eta^2 - 1}. \tag{14}$$

For $\eta = 2$, (14) becomes $M_f = 1 + 24.1K_n^2$, which agrees with numerical results in Fig 1. In Fig. 2 the mass flow rates as functions of pressure ratio η for $K_n = 0.165$ are shown for our theory, the experimental work [8], the engineering model [7] and the LBM simulation. Our theory and the LBM simulation agree well with the experimental measurements. It is noted that for large pressure ratios ($\eta \geq 1.8$), the lattice Boltzmann model agrees reasonably well with Beskok et al. [7]. But for smaller pressure ratios, the difference increases.

III. LATTICE BOLTZMANN SIMULATION OF MULTIPHASE FLOWS

Since its first being proposed as an useful alternative to classical computational fluid dynamics (CFD) techniques, the lattice Boltzmann method (LBM) has proven to be useful for simulations of multiphase flow. Instead of solving macroscopic equations such as traditional CFD approaches, the LBM simulates fluid flow based on microscopic models and mesoscopic kinetic equations. Consequently, the essential microscopic processes, such as intermolecular interactions, can be easily incorporated. Phase segregation and interfacial dynamics, which are essential in multiphase flow and are difficult to handle in traditional approaches, can be accurately simulated in the lattice Boltzmann method.

There have been several LBM models proposed for the simulation of multiphase flows. The first such model was proposed by Gunstensen et al. [9] based on a two-component lattice gas model. In this model, red and blue particle distribution functions were introduced to represent two different fluids. To maintain interfaces and to separate the different phases, an extra step was introduced to force the colored fluids to move toward fluids with the same color. The second LBM model proposed by Shan and Chen [10] used the concept of microscopic interactions between particles. An interparticle potential was introduced to model the phase segregation and surface tension. A third LBM model proposed by Swift et al. [11] used a free-energy approach. In this model, the equilibrium distribution was modified so that the pressure tensor is consistent with that derived from a free-energy function for non-uniform fluids.

Although each of the LBM multiphase models was developed based on different physical pictures and each appears to be different, a recent study [12] showed that all of them have an origin in the kinetic theory. In another words, these models can be derived by discretizing the continuous Boltzmann equation using different approximations. An improved LBM model for multiphase flows can be obtained by systematically discretizing the continuous Boltzmann equation. In this section, we report the latest development of the multiphase

model proposed by He et al. [13] and present a benchmark study of the method applied to the Rayleigh-Taylor instability.

In this new formulation of the LBM for multiphase fluid flows [13], we use an index function, f, and a pressure distribution function, g, for tracking the evolution of the multiphase fluid. The reason for using these two distributions is that, for incompressible fluids, the density is constant in each phase and only the pressure varies. In addition, if we do not follow the density field, an index function must used to track the two phases. The evolution equations for f and g are:

$$\frac{\partial f_i}{\partial t} + \mathbf{e}_i \cdot \nabla f_i = -\frac{f_i - f_i^{eq}}{\tau} + \frac{(\mathbf{e}_i - \mathbf{u}) \cdot \mathbf{F}_\tau}{RT} f_i^{eq}, \tag{15}$$

and

$$\frac{\partial g_i}{\partial t} + \mathbf{e}_i \cdot \nabla g_i = -\frac{g_i - g_i^{eq}}{\tau} + \frac{(\mathbf{e}_i - \mathbf{u}) \cdot (\mathbf{F}_d + \mathbf{F}_s + \mathbf{G})}{RT} g_i^{eq}, \tag{16}$$

where

$$\mathbf{F}_\tau = \nabla\Psi(\psi), \mathbf{F}_d = \frac{1}{\rho}\nabla(\rho RT - p), \mathbf{F}_s = \kappa\rho\nabla\nabla^2\rho, \tag{17}$$

and $\mathbf{G}$ is the gravitational force. The index function ψ, the pressure, and the velocity are calculated using:

$$\psi = \sum f_i, p = \sum g_i, p\mathbf{u} = \sum g_i \mathbf{e}_i \tag{18}$$

Ψ controls the rate of segregation of the different phases and κ controls the surface tension. The above governing equations are solved using a second-order finite differencing scheme. The equilibrium distribution functions have the Maxwellian form:

$$f_i^{eq} = \frac{\psi}{(2\pi RT)^{D/2}} \exp\left[-\frac{(\mathbf{e}_i - \mathbf{u})^2}{2RT}\right], \tag{19}$$

$$g_i^{eq} = \frac{p}{(2\pi RT)^{D/2}} \exp\left[-\frac{(\mathbf{e}_i - \mathbf{u})^2}{2RT}\right]. \tag{20}$$

For two-dimensional simulation, the discrete velocities are chosen to be the nine velocities discussed above; for three-dimensional simulations, a fifteen velocity model can be used [4].

IV. RAYLEIGH-TAYLOR INSTABILITY

When a heavy fluid is placed on top of a light fluid in a gravitational field with gravity pointing downward, the initial planar interface is unstable. Any disturbance will grow and produce spikes of heavy fluids moving downwards and bubbles of light fluids moving upwards. This is the so-called Rayleigh-Taylor instability. (For a review, see Sharp 1984 [14].)

In this study, we will focus on the Rayleigh-Taylor instability for a single-mode disturbance. The amplitude of the initial perturbation is chosen to be ten percent of the channel width. The computational domain is a two-dimensional square or three-dimensional box. Non-slip boundary conditions are applied at the top and bottom walls. Periodic boundary conditions are applied at the sides. The density ratio of heavy fluid to light fluid is 3. This corresponds to an Atwood number of 0.5. [A=$(\rho_h - \rho_l)/(\rho_h + \rho_l)$ with ρ_h and ρ_l to be densities of heavy and light fluids, respectively]. The kinetic viscosity was assumed to be the same for both heavy and light fluids. Surface tension was neglected in the simulation.

We present our results in terms of non-dimensional variables. We took the channel width W as the length scale and $T = \sqrt{W/g}$ as the time scale, where g is the gravitational acceleration. The characteristic speed is then defined as $\sqrt{AgW}$.

A. Two-dimensional simulation

A two-dimensional simulation was carried out on a 256x1024 grid. The Reynolds number, $Re = \sqrt{gW}W/\nu$ in this simulation was 2048. Fig. 3 shows the time evolution of the interface. The interface was represented by 19 equal-spaced iso-density contours. As expected, the heavy fluid forms downward spikes while the light fluid rises to form bubbles. The interface remains symmetric during the early stages of growth ($t < 1.0$). After that, the Kelvin-Helmholtz instability becomes important and the spike of the heavy fluid begins to roll up at the edges. The role-ups become quite evident at $t = 2.5$ and $t = 3.0$. Although many of the previous Rayleigh-Taylor studies stop at this time, we continues our simulation to much later times. As shown, the bubble and the front of the spike remain rather smooth and the interfaces along the edge of the spike are stretched and folded into very complicated shapes. The mixing of heavy and light fluids is considerable.

Previous theoretical and numerical studies showed that when the amplitude becomes larger than 0.4 times the wavelength, the bubble speed approaches a constant. In our study, the final bubble speed, $V_B/\sqrt{AgW}$, was found to be 0.270. This result compares well with the value of 0.265 obtained by Tryggvason using a front-tracking approach [15].

B. Three-dimensional simulation

A three-dimensional simulation was carried out on a 128x128x512 grid with a Reynolds number of 1024. Fig. 4 shows snapshots of the interface at two different time steps. The left panel is a view of the interface from the heavy fluid side, and the right panel is a view of the interface from the light fluid side. As expected, the heavy and light fluids penetrate into each other as time increases. The spike grows at about the same speed as the bubble during the early stages ($t < 1.0$), but gradually the spike becomes faster than the bubble ($t > 1.0$). The role-ups of the spike and bubble become obvious at the large-amplitude stage ($t = 3.0$). The shapes of the bubble and spike are similar to the shapes observed by Li et al. using a level set approach [16].

V. TWO-DIMENSIONAL ISOTROPIC MULTIPHASE TURBULENCE

Since there is no vortex stretching in two-dimensional Navier-Stokes, both the kinetic energy and enstrophy (vorticity squared) are conserved. Therefore, there are two cascade processes: the direct enstrophy cascade and the inverse energy cascade. A dimensional analysis can be performed for both scalings, which shows that $E(k) \sim \beta^{2/3}k^{-3}$ for the direct enstrophy cascade range and $E(k) \sim \epsilon^{2/3}k^{-5/3}$ for the inverse cascade range. Here β and ϵ are the enstrophy flux and the energy flux, respectively.

While single-phase two-dimensional turbulence has been studied extensively (See, for example, the review article by Kraichnan and Montgomery, 1980 [17]), two-phase two-dimensional immiscible turbulence is a relatively undeveloped field. Although a combined approach using both analytical theories and direct numerical simulations hao been very effective for the 2D single-phase turbulence, these methodologies cannot be extended to two-phase immiscible fluid in a straightforward manner. Conventional numerical simulations have limitations which do not permit a clear physical understanding of the interface dynamics.

In order to achieve a statistical steady state, a large-scale forcing is applied in physical space: $F_i = \mathbf{e}_i \cdot \sum_{k_{1n}^2+k_{2n}^2 \le N^2}\{k_{2n}(-A_n \sin\phi + B_n \cos\phi)\vec{i_x} + K_{1n}(A_n \sin\phi - B_n \cos\phi)\vec{i_y}\}$ with $\phi = k_{1n} \cdot x + k_{2n} \cdot y$ and $\vec{k_n} = (k_{1n}, k_{2n})$. In this way, the energy is injected into the first three modes, $N \le 3$, in physical space. Here $\vec{k}$ is the wave-vector, c is a parameter that controls the force, A_n and B_n are the random numbers in the range $[0, 1]$. This forcing is periodic and satisfies the incompressibility constraint. The boundary conditions are periodic in both directions.

To compare single-phase and two-phase turbulence in the enstrophy cascade range, we present in Fig. 5(a) the energy spectrum for a stationary state from a single-phase LBM simulation. This simulation was carried out using a 1024×1024 grid. The Taylor microscale Reynolds number, Re_λ, is about 80. Re_λ is defined as $u\lambda/\nu$, where u and λ are the root-mean-square of the velocity fluctuations and the Taylor microscale. Since the flow is forced at the largest scales, only the enstrophy cascade range is well resolved. The power law of the energy spectrum is seen for this LBM simulation to scale approximately as k^{-3} in the enstrophy cascade range. This compares well with the theoretical prediction [17].

Next, we present results from our simulations of two-dimensional two-phase immiscible fluid turbulence subject to the same forcing at large scales. The simulation was carried out using a scheme proposed by Gunstensen et al. [9] which colors the two components "red" and "blue." The viscosity and density of the two components are identical. Initially we assume that the two fluids mix completely, i.e., the density at each point is assigned to be identical. After introducing the large-scale stirring force, each component begins to move, merge and segregate due to the competition between the external forces and surface tension. Depending on the strength of the surface tension, different flow patterns appear. After the energy spectrum reaches a stationary state, the flow properties are measured. Fig. 6 illustrates the density and vorticity distribution of the two components at a late time. It is seen that, under the influence of the large-scale force and the surface tension, the two components are stretched and separated. Both large-scale and small-scale vortices are observed.

In Fig. 5(b) we present the energy spectrum of the two-phase flow. It is seen that the power law of energy spectrum is roughly $\sim k^{-2}$ in the inertial range. This result is different

from the k^{-3} behavior of single-phase turbulence and the results of Esmaeeli et al. [18]. Their energy spectrum from a low Reynolds number simulation of bubbly flows gives a larger energy decay rate. The new scaling of k^{-2} is similar to the typical scaling of the Burgers equation in which the shock structure dominates the dynamics of the velocity field. We argue that in two-phase fluid turbulence, in particular when the surface phenomenon dominates, the small scales are completely characterized by the surface velocity V and the surface thickness, $1/k$, resulting in $E(k) \sim k^{-2}$ from dimensional arguments.

VI. CONCLUDING REMARKS

In this paper, we have briefly presented the basic principles of the lattice Boltzmann method and described several applications, including the LBM simulation of the microchannel, multiphase mixing and two-dimensional multiphase turbulence. Simulation results from the LBM agree well with results from existing experimental and other numerical simulations.

We would like to emphasize that the LBM is a useful mesoscopic dynamical description of physical phenomena. The scheme is most suitable for fluid problems for which macroscopic hydrodynamics and mesoscopic statistics are both important. Even though the LBM originates from particle dynamics and uses the particle distribution function, the scheme describes the averaged macroscopic dynamics. In most cases the LBM has been treated as a numerical scheme rather than as a mesoscopic physical model. However, the utilization of the particle description or the kinetic equation provides the advantages of particle dynamics and kinetic theory, including clear physical understanding, easy boundary implementation and efficient parallel algorithms.

---

[1] S. Chen and G. D. Doolen, "Lattice Boltzmann method for fluid flows" 1998. Ann. Rev. Fluid Mech. **30**, 3294 (1998).

[2] U. Frisch, B. Hasslacher and Y. Pomeau, "Lattice gas automata for the Navier-Stokes equations," Phys. Rev. Lett. **56**, 1505 (1986).

[3] S. Chen, H. Chen, D. Martinez and W. Matthaeus, "Lattice Boltzmann model for simulation of magnetohydrodynamics," Phys, Rev. Lett. **67**, 3776 (1991)

[4] Y. H. Qian, D. d'Humières and P. Lallemand, "Lattice BGK models for Navier-Stokes equation," Europhys. Lett. **17**, 479 (1992)

[5] C. M. Ho and Y. C. Tai, "Micro-electro-mechanical-systems(MEMS) and fluid flows," Ann. Rev. Fluid Mech. 30, 579 (1998).

[6] X. Nie, G. D. Doolen and S. Chen, "Lattice Boltzmann Simulation of Fluid Flows in MEMS," submitted to Physics of Fluids, (1998).

[7] A. Beskok, G. E. Karniadakis and W. Trimmer, "Rarefaction and compressibility effects in gas micro-flows," Journal of Fluids Engineering, **118**, 448(1996).

[8] E. Arkilic, M.A. Schmidt and K.S. Breuer, "Gaseous slip flow in long micro-channels," J. MEMS **6**, 167-178(1995).

[9] A. K. Gunstensen, D. H. Rothman, S. Zaleski and G. Zanetti, "Lattice Boltzmann model of immiscible fluids," Phys. Rev. A. **43**, 4320 (1991).
[10] X. Shan and H. Chen, "Lattice Boltzmann model for simulating flows with multiple phase and components," Phys. Rev. E. **47**, 1815 (1993).
[11] M. R. Swift,W. R. Osborn and J. M. Yeomans, "Lattice Boltzmann simulation of nonideal fluids," Phys. Rev. Lett. **75**, 830 (1995).
[12] X. He, X. Shan, and G.D. Doolen, "A discrete Boltzmann equation model for non-ideal gases." *Phys. Rev. E.* **57**, R13 (1998).
[13] X. He X., R. Zhang and S. Chen, to be submitted to J. Comput. Phys. (1998).
[14] D.H. Sharp, "An overview of Rayleigh-Taylor instability," Physica D, **12**, 3 (1984).
[15] G. Tryggvason "Numerical Simulation of the Rayleigh-Taylor Instability." J. Comp. Phys. **75**, 253 (1988).
[16] X.L. Li, B.X. Jin, and J. Glimm, "Numerical study for the three-dimensional Rayleigh-Taylor instability through the TVD/AC scheme and parallel computation," J. Comp. Phys., **126**, 343 (1996).
[17] R. H. Kraichnan and D. Montgomery, "Two dimensional turbulence," Rep. Prog. Phys., **43**, 1385 (1980).
[18] A. Esmaeell, G. Tryggvason, "An inverse energy cascade in two-dimensional low Reynolds number bubbly flows," J. Fluid Mech. **314**, 315 (1996).

Figure Captions

FIG. 1. The slip velocity and the normalized mass flow rate at the exit of a micro-channel flow as functions of Knudsen number for $\eta = 2$. The "+" and "×" indicate LBM numerical results. The dashed line is for Eq.(13) and the dotted line for Eq.(14).

FIG. 2. The normalized mass flow rate as a function of pressure ratio for $K_n = 0.165$. The solid line is for Eq.(14).

FIG. 3. Time-evolution of the interface for the two-dimensional Rayleigh-Taylor instability. The Atwood number is 0.5, the Reynolds number is 2048 and the viscosity ratio is 1. Surface tension is neglected.

FIG. 4. Interface shapes at two times in three-dimensional Rayleigh-Taylor instability. The Atwood number is 0.5, the Reynolds number is 1024 and the viscosity ratio is 1. Surface tension is neglected. The left panel is a view of the interface from the heavy fluid side, and the right panel is a view of the interface from the light fluid side. The upper row is at $t = 1.0$ and the lower row is at $t = 3.0$.

FIG. 5. Energy spectrum for the two-dimensional forced single-phase (a) and two-phase (b) turbulence.

FIG. 6. The density distribution of the two-dimensional forced immiscible two-phase turbulence.

Fig.1

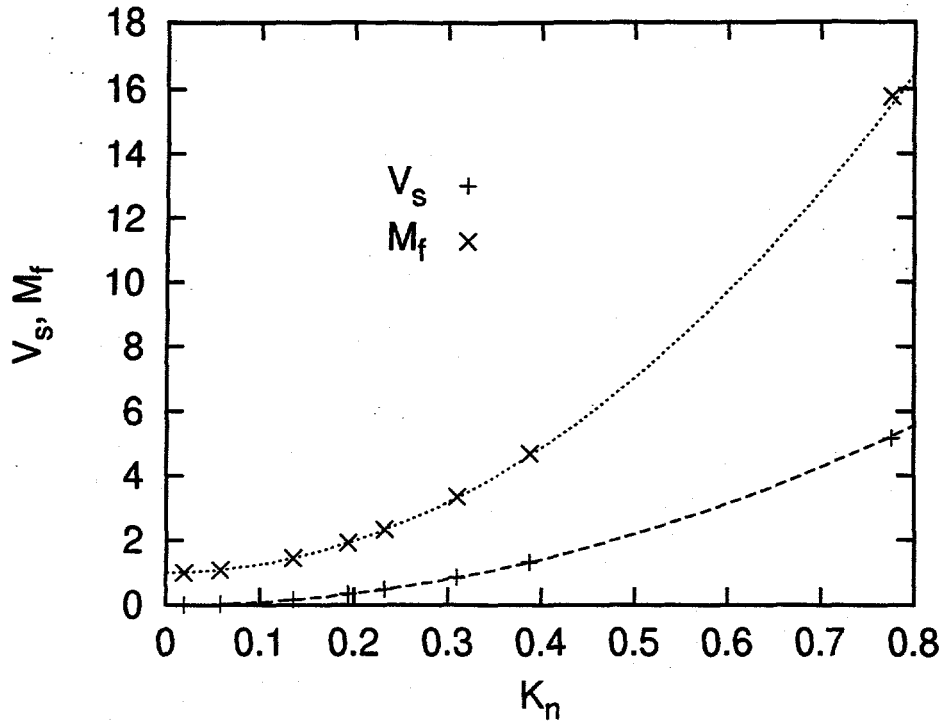
18
16
14
12
10
8
6
4
2
0
0
0.1
0.2
0.3
0.4
0.5
0.6
0.7
0.8
V_s +
M_f ×
V_s, M_f
K_n

Fig.2

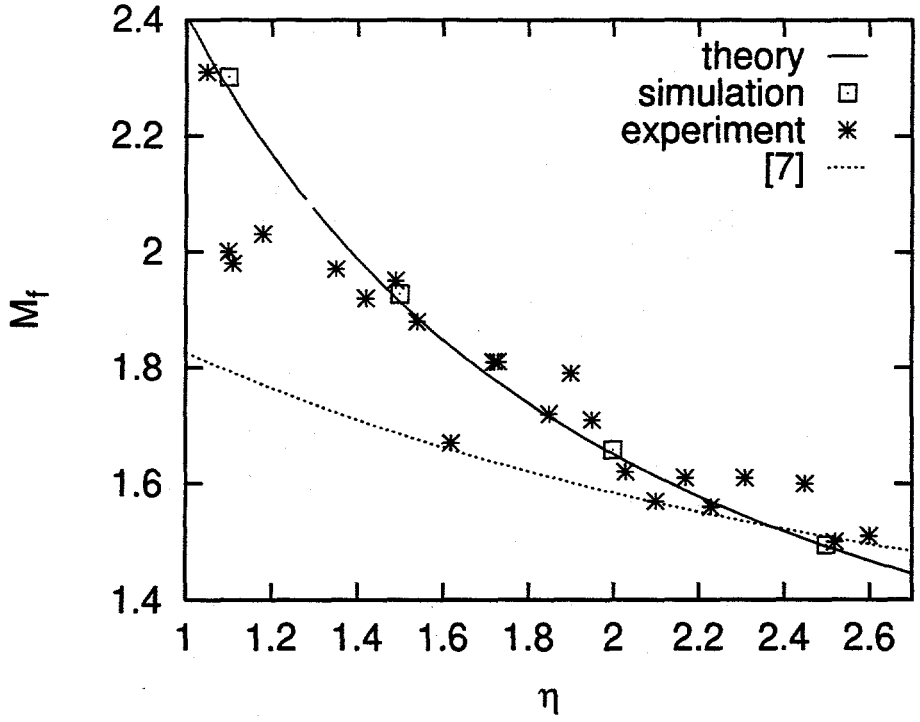
2.4
2.2
2
1.8
1.6
1.4
1
1.2
1.4
1.6
1.8
2
2.2
2.4
2.6
theory
simulation
experiment
[7]
M_f
η

Fig.3

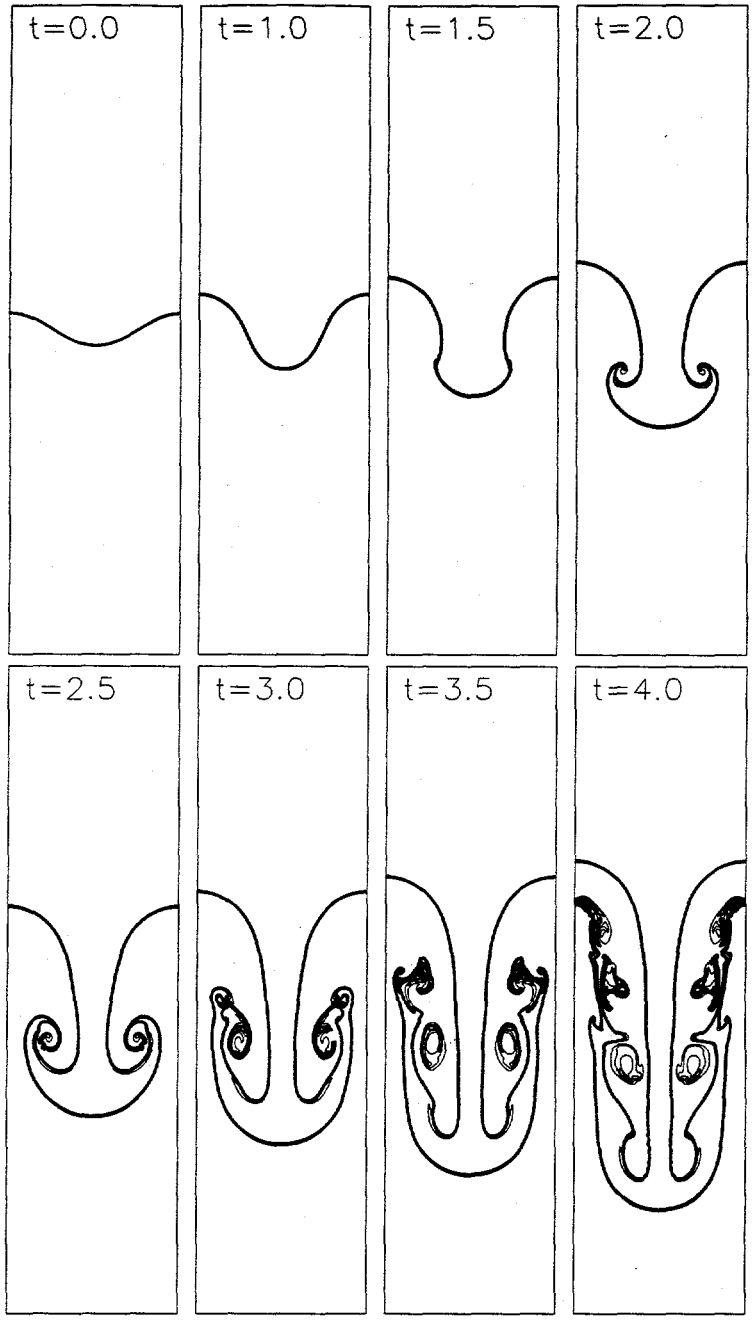

Fig.4

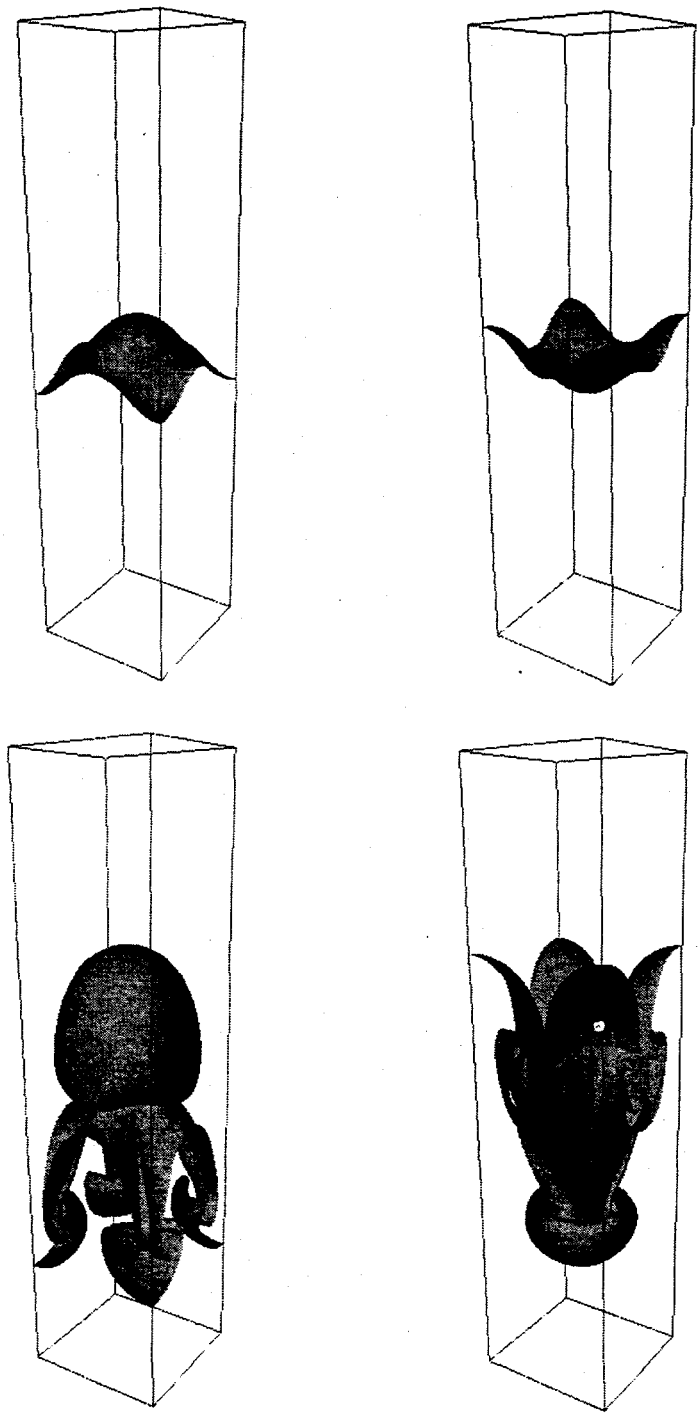

Fig. 5

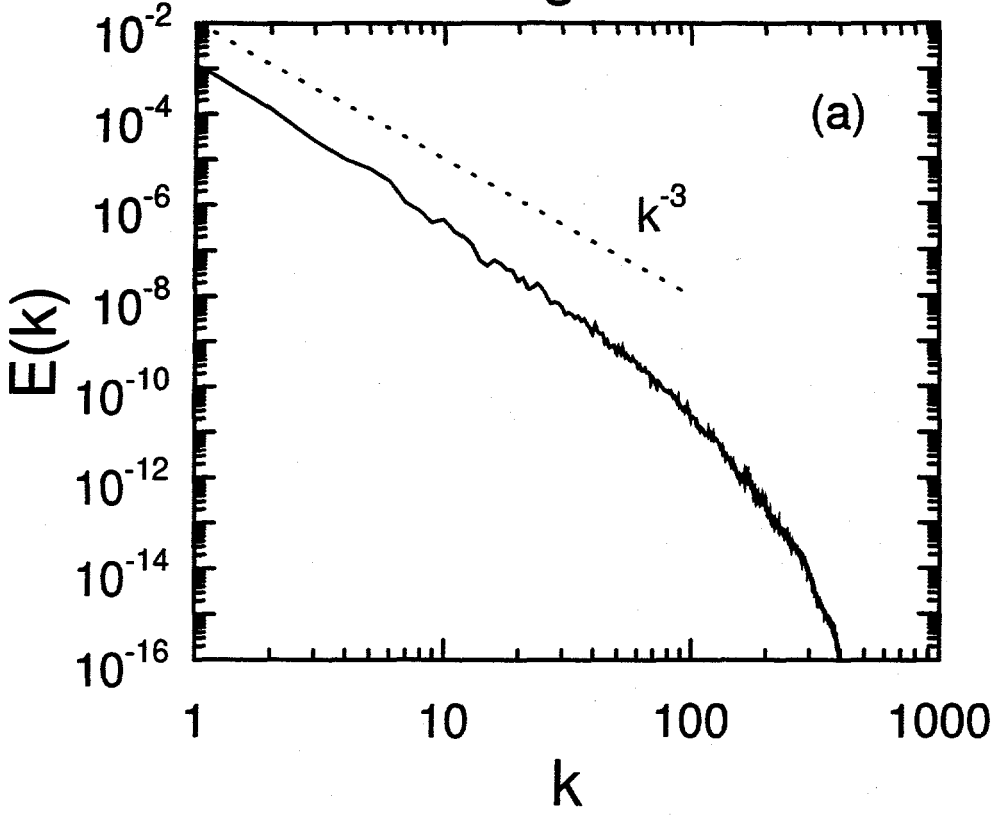
10^-2
10^-4
10^-6
10^-8
10^-10
10^-12
10^-14
10^-16
E(k)
(a)
k^-3
1
10
100
1000
k

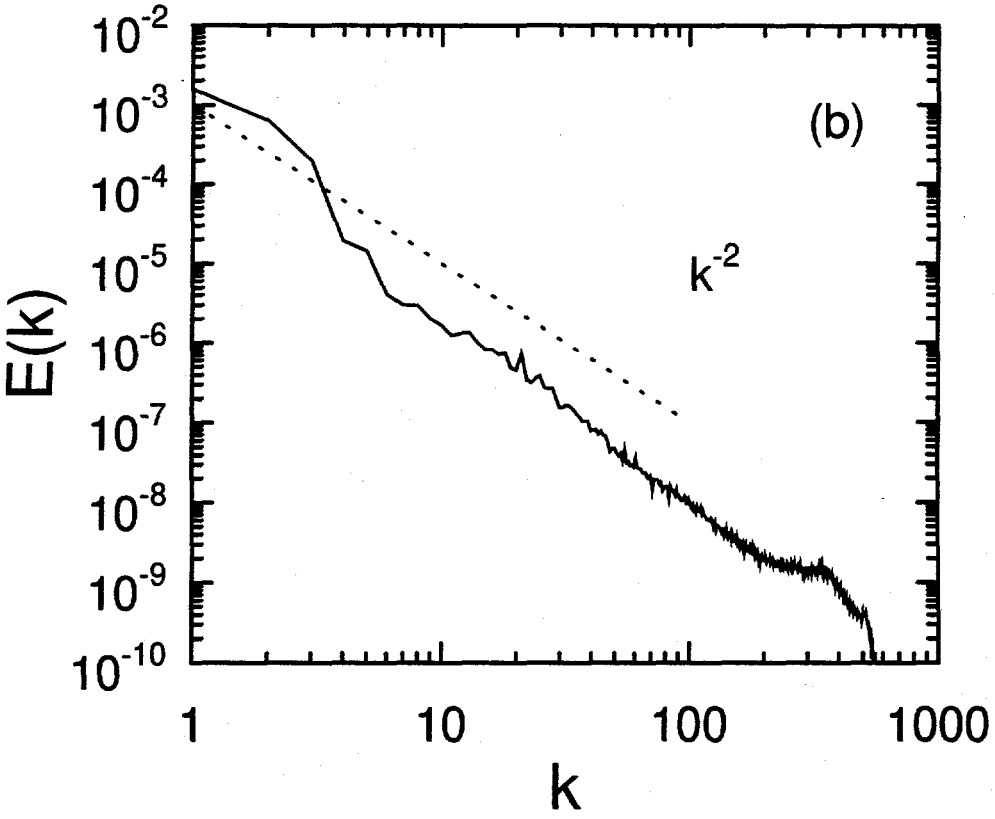
10^-2
10^-3
10^-4
10^-5
10^-6
10^-7
10^-8
10^-9
10^-10
E(k)
(b)
k^-2
1
10
100
1000
k

Fig. 6